ACS APPLIED MATERIALS & INTERFACES

Research Article

www.acsami.org

Comparison of the Photovoltaic Response of Oleylamine and Inorganic Ligand-Capped $CuInSe_2$ Nanocrystals

C. Jackson Stolle, Matthew G. Panthani, Taylor B. Harvey, Vahid A. Akhavan, and Brian A. Korgel*

Department of Chemical Engineering, Texas Materials Institute, and Center for Nano- and Molecular Science and Technology, The University of Texas at Austin, Austin, Texas 78712-1062, United States

ABSTRACT: Thin film photovoltaic devices (PVs) were fabricated with $CuInSe_2$ (CIS) nanocrystals capped with either oleylamine, inorganic metal chalcogenide-hydrazinium complexes (MCC), or S^{2-}, HS^-, and OH^-. A CIS nanocrystal layer deposited from solvent-based inks without high temperature processing served as the active light-absorbing material in the devices. The MCC ligand-capped CIS nanocrystal PVs exhibited power conversion efficiency under AM1.5 illumination (1.7%) comparable to the oleylamine-capped CIS nanocrystals (1.6%), but with significantly thinner absorber layers. S^{2-}-capped CIS nanocrystals could be deposited from aqueous dispersions, but exhibited lower photovoltaic performance.

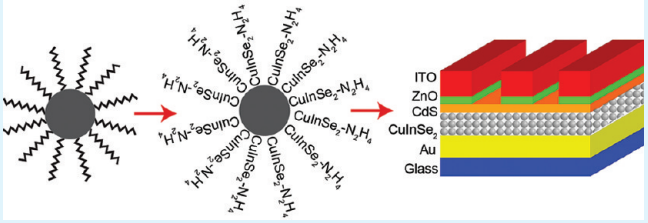

KEYWORDS: *$CuInSe_2$, Metal Chalcogenides, nanocrystals, photovoltaics, solar cells*

INTRODUCTION

There is an active search to identify semiconductor nanocrystals for photovoltaic devices (PVs) with low cost and high efficiency. Nanocrystals represent an alternative to organic PV materials, as they can be synthesized in industrial-scale quantities, dispersed and handled in solvents, and deposited easily on large-area substrates, with potentially better air- and photostability and higher performance. To date, the highest reported efficiency under AM 1.5 illumination from a nanocrystal-based PV without high temperature processing is just over 6% using PbS nanocrystals.[1,2] PVs using PbSe,[3−7] Cu_2S,[8] CdTe,[9,10] and $Cu(In_{1-x}Ga_x)Se_2$ (CIGS)[11,12] nanocrystals have achieved efficiencies in the range of 1−5%. Higher device efficiencies, even exceeding 10%, have been achieved by high temperature sintering of CdTe,[13] $Cu(In_{1-x}Ga_x)Se_2$,[14] $Cu(In_{1-x}Ga_x)S_2$,[15] and Cu_2ZnSnS_4[16] nanocrystal films for improved electrical transport and charge extraction. High temperature sintering, however, adds significant cost and eliminates a variety of different substrate choices, including cheap plastic substrates with low melting temperature like polyethylene. The ideal materials would enable high efficiency (>10% PCE) without postdeposition thermal processing. One thought is that the capping ligands on the nanocrystals might be engineered and optimized for efficient performance.

Nanocrystals are typically synthesized using organic capping ligands to stabilize their size and prevent aggregation, but the ligands create a barrier to charge transport that limits PV device performance.[17,18] By exchanging organic ligands in PbS and PbSe nanocrystal films with hydrazine (PbSe),[3,19] benzenedithiol (PbSe),[4,5] and halide ions (PbS),[1] considerable enhancements of PV device performance have been achieved. Layers of CdSe nanocrystals capped with metal-free inorganic ligands (i.e., $(NH_4)_2S$)[20] or metal chalcogenide complexes (MCCs) have exhibited very high carrier mobilities—of more than 10 $cm^2/(V\ s)$ for MCC-capped nanocrystals.[21−24] Although these results hint at the general application of inorganic ligands for higher performance nanocrystal-based PVs, there have actually been no reports of PVs made with inorganic ligand-capped nanocrystals deposited directly from solution, or enhancements in PV devices made with nanocrystals other than Pb-chalcogenides. If high carrier mobilities, such as those observed from CdSe nanocrystals, are actually trap-related it may not be possible to use them in PVs. Therefore, we sought to determine the viability of inorganic ligands toward improving the efficiency of PVs made with $CuInSe_2$ (CIS) nanocrystals.

We have achieved reasonable device efficiency (2−3%) using oleylamine-capped CIS nanocrystals without high temperature postdeposition processing,[18] and therefore use these materials as a benchmark to compare devices with CIS nanocrystals capped with inorganic MCC ligands. The devices made from MCC-capped CIS nanocrystals worked, and exhibited similar performance as those made with oleylamine-capped CIS nanocrystals, but using significantly thinner nanocrystal layers.

EXPERIMENTAL METHODS

Chemicals. Copper(I) chloride (CuCl, 99.99%), elemental selenium (Se, 99.99%), copper(II) sulfide (CuS, 99.99%), indium(III) selenide (In_2Se_3, 99.99%), elemental sulfur (S, 99.98%), sodium sulfide nonahydrate ($Na_2S{\cdot}9H_2O$, 99.99%), cadmium sulfate ($CdSO_4$, 99.99%), thiourea (99%), anhydrous hydrazine (98%), anhydrous toluene (99.8%), anhydrous ethanol (99.5%), and anhydrous acetonitrile (99.8%) were obtained from Aldrich; indium(III) chloride ($InCl_3$, 99.99%) was obtained from Strem Chemical; oleylamine

Received: March 1, 2012
Accepted: April 23, 2012
Published: April 23, 2012

dx.doi.org/10.1021/am3003846 | ACS Appl. Mater. Interfaces 2012, 4, 2757−2761

(>40%) was obtained from TCI America; toluene, ethanol, hexanes, and ammonium hydroxide (18 M NH_4OH) were obtained from Fisher Scientific. Oleylamine was degassed by pulling vacuum overnight at ~200 mTorr at 110 °C and stored in an N_2 filled glovebox before use. Anhydrous hydrazine was distilled and stored inside an N_2 filled glovebox to prevent a possible explosion. Hydrazine is a highly toxic and explosive chemical, and all work with hydrazine was conducted inside of a N_2 filled glovebox. All other chemicals were used as received.

$CuInSe_2$ Nanocrystal Synthesis. CIS nanocrystals were synthesized using a modification of published procedures.[12] In a typical reaction, 2 mmol of CuCl, 2 mmol of $InCl_3$, 4 mmol of Se, and 20 mL of degassed oleylamine are added to a 100 mL three-neck flask inside an N_2 filled glovebox. The flask is attached to a standard Schlenk line and degassed at 110 °C under a vacuum for 45 min. The flask is then filled with nitrogen and heated to 200 °C. After 30 min, the temperature is raised to 260 °C. After 10 min, the heating mantle is removed and the reaction is allowed to cool to room temperature. The nanocrystals are washed via centrifugation using toluene and ethanol as the solvent and antisolvent, respectively. Poorly capped nanocrystals are then separated from the toluene solution via centrifugation. The final nanocrystal dispersion is then transferred to a glovebox for the ligand exchange.

Metal Chalcogenide Complex Preparation. MCCs of metal chalcogenide anions complexed with hydrazinium ($N_2H_5^+$)[25−29] were formed by dissolving metal and chalcogen in hydrazine following the procedures of Kovalenko et al.[21] A 0.25 M solution of $N_4H_9Cu_7S_4$ (Cu_2S-MCC) was prepared by dissolving 2.5 mmol of Cu_2S powder in 7.5 mL of hydrazine and adding 2.5 mL of 1 M S solution in hydrazine. A 0.25 M solution of $(N_2H_4)_2(N_2H_5)_2In_2Se_4$ (In_2Se_3-MCC) was prepared by dissolving 2 mmol of In_2Se_3 powder in 4 mL of hydrazine and adding 4 mL of 1 M Se solution in hydrazine. A 0.25 M solution of $(N_2H_4)_x(N_2H_5)_3(Cu_2In_2S_3Se_4)$ (CIS-MCC ligand) was prepared by mixing equal volumes of the 0.25 M In_2Se_3-MCC and 0.25 M Cu_2S-MCC solutions. The solutions are filtered (0.25 μm PTFE syringe filter) before use.

Oleylamine/MCC Ligand Exchange. 0.25 mL of 0.25 M MCC stock solution (in hydrazine), 10 mL of hydrazine and 5 mL of CIS nanocrystals dispersed in toluene at a concentration of 200 mg/mL were combined and stirred for two days. The nanocrystals transfer from the toluene phase to the hydrazine phase. The nanocrystals were isolated from the hydrazine phase by precipitation with ~4 mL of acetonitrile and centrifugation (8000 rpm, 2 min). The nanocrystals were redispersed in 5 mL of hydrazine. Five milliliters of toluene were added and the vial was mixed to remove any residual oleylamine. The hydrazine phase was again decanted and the nanocrystals washed with the acetonitrile/hydrazine antisolvent/solvent combination.

Oleylamine ligands were exchanged with S^{2-}, HS^-, and OH^- ions as described by Nag et al.[16] 0.8 g of $Na_2S{\cdot}9H_2O$ was dissolved in 20 mL of DI water. Five milliliters of a toluene dispersion of CIS nanocrystals (200 mg/mL) were added to the aqueous Na_2S solution and stirred overnight. The majority of the nanocrystals transfer from the toluene phase to the water phase. The nanocrystals were precipitated by adding 20 mL of acetone and centrifuging at 8000 rpm for 3 min. The S^{2-}, HS^-, and OH^- capped (collectively, Na_2S-capped) nanocrystals were redispersed in 5 mL of DI water. Residual organics are removed by adding hexanes and decanting the mixture three times.

Materials Characterization. Nanocrystals were characterized by transmission electron microscopy (TEM) using either a Phillips 208 TEM operated at 80 kV accelerating voltage or a JEOL 2010F TEM at 200 kV accelerating voltage. TEM samples were prepared by drop-casting dilute nanocrystal dispersions in chloroform or water onto a 200 mesh nickel grid with a continuous carbon film (Electron Microscopy Sciences). Scanning electron microscopy (SEM) was performed on a Zeiss Supra 40 VP SEM operated at 5 keV accelerating voltage through an In-lens detector with samples grounded using copper tape.

X-ray diffraction (XRD) was performed using a Rigaku R-Axis Spider diffractometer with an image-plate detector and Cu Kα (λ = 1.54 Å) radiation operated at 40 kV and 40 mA. XRD samples were prepared by drying a drop of concentrated nanoparticle dispersion onto a glass slide in a glovebox. The nanocrystal powder was then suspended on a 0.5 mm nylon loop using mineral oil for analysis. Samples were scanned for 15 min while rotating at 2°/s The 2D diffraction patterns were integrated using the Rigaku 2DP powder processing suite with subtraction of the background scattering from the nylon loop and mineral oil.

UV−vis−NIR absorbance spectra were acquired with a Varian Cary 500 UV−vis−NIR spectrophotometer. Oleylamine-capped CIS nanocrystals were dispersed in toluene and MCC- and Na_2S-capped nanocrystals were dispersed in water. Measurements were performed at room temperature in quartz cuvettes.

CIS Nanocrystal PV Device Fabrication and Testing. CIS nanocrystal PVs were fabricated with a Au/CIS/CdS/i-ZnO/indium tin oxide (ITO) device structure. A 5 nm layer of Cr followed by 60 nm of Au were thermally deposited onto soda lime glass (Delta Technologies, 25 mm × 25 mm × 1.1 mm polished float glass). Films of CIS nanocrystals were then deposited. Oleylamine-capped nanocrystals were spray deposited from toluene at room temperature as described previously.[13] Na_2S-capped nanocrystals were spray deposited from water onto substrates heated to 100 °C. MCC-capped nanocrystals dispersed in hydrazine were deposited by a spin-coating procedure inside an N_2 filled glovebox. A layer of MCC-capped nanocrystals was deposited by dropping 70 μL of nanocrystal/hydrazine dispersion onto the substrate and rotating at 2000 rpm for 90 s to spread and dry the film. The substrate was then heated to 150 °C on a hot plate for 5 min prior to depositing the next layer of nanocrystals. This spin coating procedure was repeated 1−4 times. A CdS buffer layer was deposited by dropping 0.7 mL of a CdS precursor solution (1.25 mL of 15 mM $CdSO_4$, 2.2 mL of 1.5 M thiourea, and 2.8 mL of 18 M NH_4OH in water) onto the CIS nanocrystal film heated to 80 °C on a hot plate and covered with an inverted crystallization dish for 2 min.[30] The substrate was removed from the hot plate, rinsed with DI water, and dried with a stream of compressed air. Top layers of i-ZnO and ITO were deposited by RF sputtering from a ZnO target (Lesker, 99.9%) in a 0.5% O_2 in Ar atmosphere (Praxair, 99.95%) and a ITO target (Lesker, 99.99% In_2O_3:SnO_2 90:10) in Ar atmosphere (Praxair, research grade). ZnO and ITO are deposited selectively onto 8 rectangular regions with active device areas of 0.08 cm^2. Silver paint was applied for electrical contact to the devices. Prior to the device measurements, the completed devices were placed in a vacuum oven for 10 min at 200 °C to improve the conductivity of the ITO.

PV device response was measured using a Keithley 2400 General Purpose Sourcemeter under solar simulation using a Newport Xenon Lamp Solar Simulator with an AM1.5 filter (100 mW/cm^2). Incident photon conversion efficiency (IPCE) was measured using a home-built device with lock-in amplifier (Stanford Research Systems, model SR830) and monochromator (Newport Cornerstone 260 1/4M), and calibrated with Si and Ge photodiodes (Hamamatsu).

RESULTS AND DISCUSSION

Oleylamine-Capped $CuInSe_2$ (CIS) Nanocrystals before and after Inorganic Ligand Exchange. Figure 1 shows TEM images of CIS nanocrystals made with oleylamine capping ligands before and after Na_2S and CIS-MCC ligand exchange. The nanocrystals have an average diameter of about 12 nm. TEM and XRD (Figure 2) confirmed that the particles are crystalline before and after ligand exchange with no observable change in crystal structure. The optical properties of the nanocrystals are also unaffected by the ligand exchange, with similar absorbance spectra before and after ligand exchange (Figure 3). However, the inorganic ligand-capped nanocrystals are more prone to agglomeration (Figure 1c−f) and are not as easily deposited into thin films as the oleylamine-capped nanocrystals. Furthermore, the need for hydrazine to disperse the CIS-MCC capped nanocrystals severely limits the

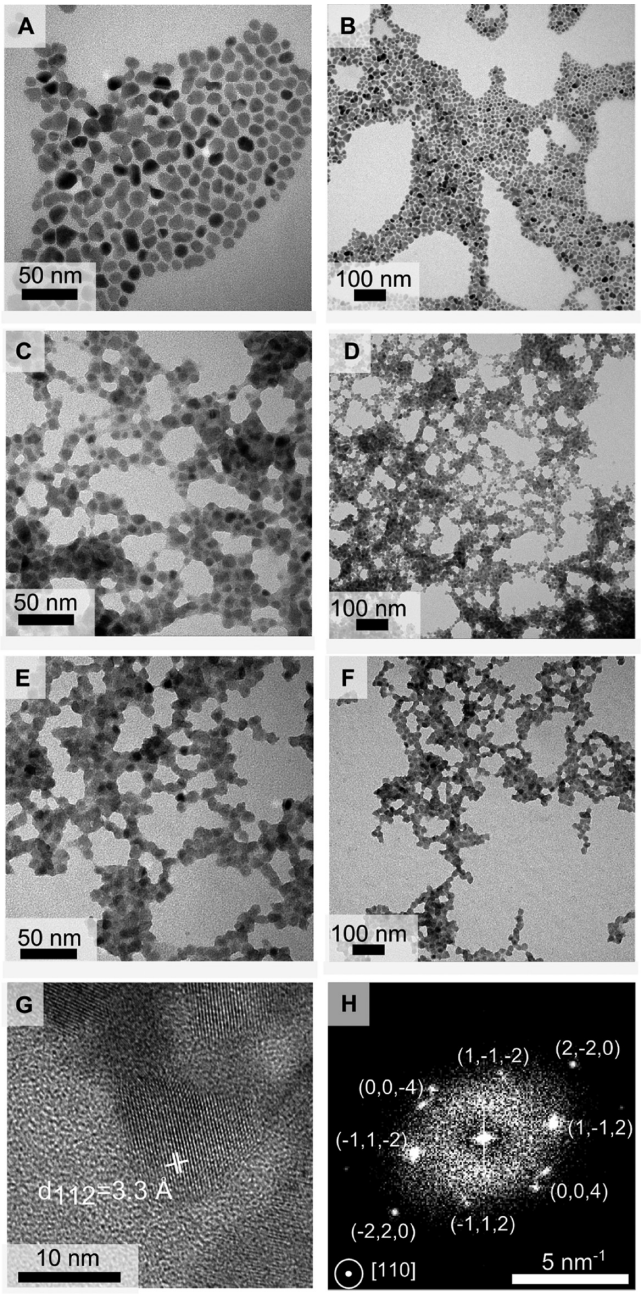

Figure 1. TEM images of CIS nanocrystals: (a, b) synthesized with oleylamine capping ligands and ligand exchanged with (c, d) Na_2S and (e, f) CIS-MCC. (g) High-resolution TEM image and (h) corresponding FFT of a CIS nanocrystal after oleylamine ligand exchange with CIS-MCC. The nanocrystal is imaged down the [110] crystallographic zone axis and the FFT is indexed to chalcopyrite CIS. The measured *d*-spacing is d_{112} = 3.3 Å.

methods that can be used to deposit uniform films onto substrates.

CIS Nanocrystal Film Deposition. For device fabrication, the oleylamine-capped CIS nanocrystals are dispersed in toluene (~20 mg/mL) and then spray-deposited into a uniform layer approximately 200 nm thick.[13] The Na_2S-capped CIS nanocrystals disperse in water and could also be spray-deposited, but the substrate needs to be heated to achieve uniform film thickness due to the low volatility of the solvent. The low solvent volatility made it difficult to deposit thicker films, and even with heating of the substrate it was not possible

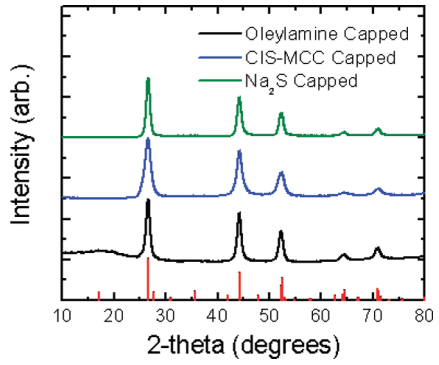

Figure 2. XRD patterns from CIS nanocrystals synthesized with oleylamine capping ligands before (black) and after exchange with CIS-MCC ligand (blue) or Na_2S (green). The red reference lines correspond to chalcopyrite CIS (PDF #97−006−892). The absence of the (112) peak indicates that there may be Cu and In positional disorder.

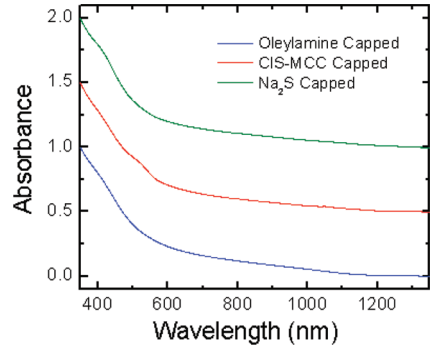

Figure 3. Optical absorbance spectra of as-synthesized oleylamine-capped CIS nanocrystals (blue) and CIS nanocrystals after ligand exchange with CIS-MCC ligands (red) and Na_2S (green). Spectra are offset by 0.5 absorbance units for clarity.

to increase the thickness of the Na_2S-capped CIS nanocrystal films above about 75 nm while retaining a uniform film thickness. The MCC-capped CIS nanocrystals are dispersible in hydrazine and other polar solvents, like dimethyl sulfoxide, and water. Films of MCC-capped CIS nanocrystals could be sprayed from dispersions in dimethyl sulfoxide and water, but devices using these layers performed extremely poorly. Only when the MCC-capped CIS nanocrystals were deposited from hydrazine could PV devices with reasonable response be made. Unfortunately, nanocrystals dispersed in hydrazine cannot be spray-deposited due to the very high toxicity of hydrazine and its potential instability (i.e., explosiveness). Therefore, the MCC-capped CIS nanocrystals were spin-coated onto the device substrates, which ultimately limited the thickness of the nanocrystal films to about 75 nm.

Figure 4 shows SEM images of films of CIS nanocrystals capped with CIS-MCC ligands. The SEM images show that the nanocrystal film is relatively uniform in density with a nanocrystalline morphology—there is no particle sintering or grain growth due to film heating on the hot plate. The cross-sectional SEM image of a CIS-MCC-capped nanocrystal device shows the lateral uniformity of the nanocrystal film and the relative thicknesses of the device layers.

PV Device Performance. The PV response and IPCE for devices made with oleylamine-capped, CIS-MCC ligand-capped, and Na_2S-capped CIS nanocrystals are shown in

dx.doi.org/10.1021/am3003846 | ACS Appl. Mater. Interfaces 2012, 4, 2757−2761

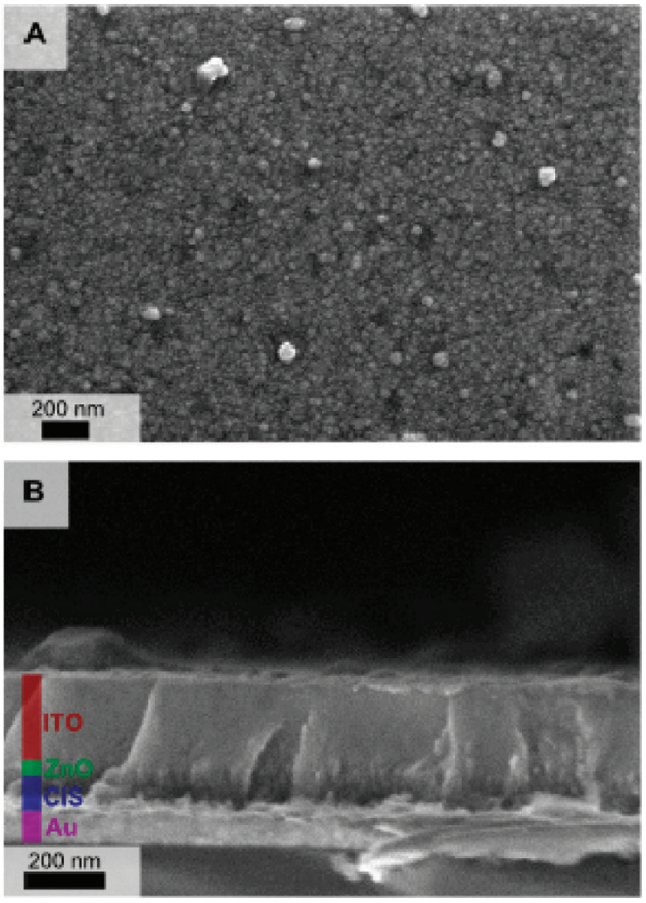

Figure 4. SEM images of (a) the surface of a spin-coated CIS nanocrystal film and (b) a cross-sectioned PV device with a layer of CIS-MCC ligand-capped CIS nanocrystals. The Au, CIS-MCC nanocrystal, ZnO and ITO layers are 70, 75, 40, and 200 nm thick, respectively.

Figure 5. The efficiency of the best CIS-MCC ligand-capped CIS device (1.68%) is similar to the best oleylamine-capped CIS device (1.56%). The best efficiency for a Na_2S-capped CIS device was significantly lower than the devices made with either oleylamine-capped or MCC-capped CIS nanocrystals, but the devices worked, demonstrating that it may be possible to fabricate reasonable PV devices under ambient conditions using water as a solvent with further optimization. Devices were fabricated with other MCC-capped CIS nanocrystals as well, and the device characteristics are listed in Table 1.

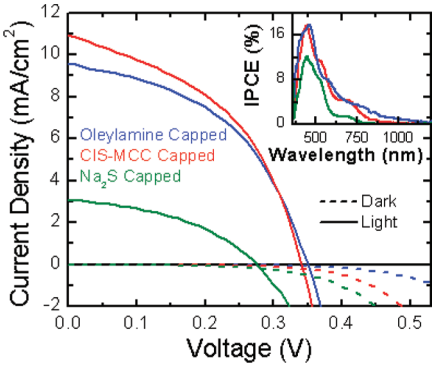

Figure 5. Dark and light $J-V$ characteristics under AM1.5 illumination (100 mW/cm^2) for the highest performance devices fabricated using oleylamine-capped CIS nanocrystals (blue; PCE = 1.56%), CIS-MCC ligand-capped CIS nanocrystals (red; PCE = 1.68%), and Na_2S-capped CIS nanocrystals (green; PCE = 0.35%). The dashed lines are the dark $J-V$ characteristics and the solid lines are the light $J-V$ characteristics. IPCE measurements for each device are shown in the inset. The active device area is 0.08 cm^2.

Table 1. Characteristics of PV Devices Fabricated with CIS Nanocrystals Capped with Various Ligands

ligand	PCE (%)	V_{oc} (V)	J_{sc} (mA/cm^2)	FF	R_s (Ω)	R_{sh} (MΩ)
oleylamine	1.56	0.349	9.59	0.467	69.0	0.92
Cu_2S-MCC	1.42	0.396	7.76	0.461	7.65	1.00
CIS-MCC	1.68	0.340	10.96	0.450	6.46	0.36
Na_2S	0.35	0.274	3.10	0.416	11.6	0.09

The wavelength dependence of the IPCE data mirrors the absorbance spectra of the CIS nanocrystals, confirming that the CIS nanocrystals are the active light-absorbing material in the device. The absorption edge extends into the near-infrared toward the CIS band gap of 1.0 eV.[31] The peaking of the IPCE at shorter wavelength (<600 nm) results from the increased light absorption from CIS in that wavelength range. CdS does absorb light at energy above its band gap of 2.42 eV (510 nm), but contributes little to the IPCE, as the CdS layer in the device is very thin relative to the nanocrystal layer and absorbs less than 25% of the total incident photons at 400 nm.

On average, the performance of devices made with MCC-capped CIS nanocrystals was more consistent with fewer shorted devices than the oleylamine-capped CIS nanocrystals. Furthermore, the series resistance R_s, of the devices was consistently lower for the devices with inorganic-capped CIS nanocrystals. Table 1 lists the values of R_s and the shunt resistance R_{sh} of the best devices estimated by fitting the dark $J-V$ curves to the diode equation,

$$J = J_0\left[\exp\left(\frac{V - IR_s}{nkT}\right) + \left(\frac{V - IR_s}{J_0AR_{sh}}\right) - 1\right] \quad (1)$$

J is the current density, J_0 is the saturation current density under reverse bias, n is the ideality factor of the device, k is Boltzmann's constant, and T is the temperature.

Although the MCC-capped and oleylamine-capped CIS nanocrystal PVs exhibited comparable power conversion efficiency, the MCC-capped nanocrystal layers in the devices were much thinner than the oleylamine-capped nanocrystal layers, implying that the internal quantum efficiency of the MCC-ligand capped nanocrystal devices may be higher. At the moment, we have not been able to increase the thickness of the MCC-ligand capped nanocrystals because they must be spin-coated under carefully controlled environmental conditions because of the hazardous nature of hydrazine. Additionally, these spin-coated layers are often streaky and nonuniform. The need for hydrazine represents a bottleneck to using these nanocrystals in PVs. New solvents and deposition techniques need to be explored in order to improve PV efficiency and deposit thicker, uniform films under ambient conditions.

CONCLUSIONS

The device results presented here prove that it is possible to use inorganic capping moieties for nanocrystal-based PVs. The device efficiencies are still relatively low, at about 2% PCE

under AM1.5 illumination, so it is still unclear if the use of inorganic ligands will yield the needed boost in device efficiency without resorting to high temperature sintering, but undoubtedly MCC-capped nanocrystals can yield PV response. One of the biggest problems with the metal chalcogenide complexes is the need to use hydrazine as a solvent. With this limitation, commercial application may not be possible. Therefore, the device results from the inorganic capped CIS nanocrystals using water as a solvent are encouraging, even though the performance was substantially less.

AUTHOR INFORMATION

Corresponding Author

*E-mail: korgel@che.utexas.edu. Tel: +1-512-471-5633. Fax: +1-512-471-7060.

Notes

The authors declare no competing financial interest.

ACKNOWLEDGMENTS

Financial support of this work was provided by the Robert A. Welch Foundation (F-1464), the Air Force Research Laboratory (FA-8650-07-2-5061), and the NSF Industry/University Cooperative Research Center on Next Generation Photovoltaics (IIP-1134849).

REFERENCES

(1) Tang, J.; Kemp, K. W.; Hoogland, S.; Jeong, K. S.; Liu, H.; Levina, L.; Furukawa, M.; Wang, X.; Debnath, R.; Cha, D.; Chou, K. W.; Fischer, A.; Amassian, A.; Asbury, J. B.; Sargent, E. H. *Nat. Mater.* **2011**, *10*, 765−771.

(2) Pattantyus-Abraham, A. G.; Kramer, I. J.; Barkhouse, A. R.; Wang, X.; Konstantatos, G.; Debnath, R.; Levnia, L.; Raabe, I.; Nazeeruddin, M. K.; Grätzel, M.; Sargent, E. H. *ACS Nano* **2010**, *4* (6), 3374−3380.

(3) Semonin, O. E.; Luther, J. M.; Choi, S.; Chen, H.-Y.; Gao, J.; Nozik, A. J.; Beard, M. C. *Science* **2011**, *334*, 1530−1533.

(4) Ma, W.; Swisher, S. L.; Ewers, T.; Engel, J.; Ferry, V. E.; Atwater, H. A.; Alivisatos, A. P. *ACS Nano* **2011**, *5* (10), 8140−8147.

(5) Ouyang, J.; Schuurmans, C.; Zhang, Y.; Nagelkerke, R.; Wu, X.; Kingston, D.; Wang, Z. Y.; Wilkinson, D.; Li, C.; Leek, D. M.; Tao, Y.; Yu, K. *ACS Appl. Mater. Interfaces* **2011**, *3* (2), 553−565.

(6) Choi, J. J.; Lim, Y.-F.; Santiago-Berrios, M. B.; Oh, M.; Hyun, B.-R.; Sun, L.; Bartnik, A. C.; Goedhard, A.; Malliaras, G. G.; Abruña, H. D.; Wise, F. W.; Hanrath, T. *Nano Lett.* **2009**, *9*, 3749−3755.

(7) Szendrei, K.; Gomulya, W.; Yarema, M.; Heiss, W.; Loi, M. A. *Appl. Phys. Lett.* **2010**, *97*, 203501.

(8) Wu, Y.; Wadia, C.; Ma, W.; Sadtler, B.; Alivisatos, A. P. *Nano Lett.* **2008**, *8*, 2551−2555.

(9) Olson, J. D.; Rodriguez, Y. W.; Yang, L. D.; Alers, G. B.; Carter, S. A. *Appl. Phys. Lett.* **2010**, *96*, 242103.

(10) Gur, I.; Fromer, N. A.; Geier, M. L.; Alivisatos, A. P. *Science* **2005**, *310*, 462−465.

(11) Panthani, M. G.; Akhavan, V.; Goodfellow, B.; Schmidtke, J. P.; Dunn, L.; Dodabalapur, A.; Barbara, P. F.; Korgel, B. A. *J. Am. Chem. Soc.* **2008**, *130*, 16770−16777.

(12) Akhavan, V. A.; Goodfellow, B. W.; Panthani, M. G.; Reid, D. K.; Hellebusch, D. J.; Adachi, T.; Korgel, B. A. *Energy Environ. Sci.* **2010**, *3*, 1600−1606.

(13) Jasieniak, J.; MacDonald, B. I.; Watkins, S. E.; Mulvaney, P. *Nano Lett.* **2011**, *11*, 2856−2864.

(14) Guo, Q.; Kim, S. J.; Kar, M.; Shafarman, W. N.; Birkmire, R. W.; Stach, E. A.; Agrawal, R.; Hillhouse, H. W. *Nano Lett.* **2008**, *8*, 2982−2987.

(15) Guo, Q.; Ford, G. M.; Yang, W.-C.; Walker, B. C.; Stach, E. A.; Hillhouse, H. W.; Agrawal, R. *J. Am. Chem. Soc.* **2010**, *132*, 17384−17386.

(16) Guo, Q.; Ford, G. M.; Hillhouse, H. W.; Agrawal, R. *Nano Lett.* **2009**, *9*, 3060−3065.

(17) Talapin, D. V.; Lee, J.; Kovalenko, M. V.; Shevchenko, E. V. *Chem. Rev.* **2010**, *110*, 389−458.

(18) Akhavan, V. A.; Panthani, M. G.; Goodfellow, B. W.; Reid, D. K; Korgel, B. A. *Optics Express* **2010**, *18*, A411−A420.

(19) Law, M.; Luther, J. M.; Song, Q.; Hughes, B. K.; Perkins, C. L.; Nozik, A. J. *J. Am. Chem. Soc.* **2008**, *130*, 5974.

(20) Nag, A.; Kovalenko, M. V.; Lee, J.-S.; Liu, W.; Spokoyny, B.; Talapin, D. V. *J. Am. Chem. Soc.* **2011**, *133*, 10612−10620.

(21) Kovalenko, M. V.; Scheele, M.; Talapin, D. V. *Science* **2009**, *324*, 1417−1420.

(22) Kovalenko, M. V.; Badnarchuk, M. I.; Zaumseil, J.; Lee, J.-S.; Talapin, D. V. *J. Am. Chem. Soc.* **2010**, *132*, 10085−10092.

(23) Kovalenko, M. V.; Bodnarchuk, M. I.; Talapin, D. V. *J. Am. Chem. Soc.* **2010**, *132*, 15124−15126.

(24) Lee, J.-S.; Kovalenko, M. V.; Huang, J.; Chung, D. S.; Talapin, D. V. *Nat. Nanotechnol.* **2011**, *6*, 348−352.

(25) Mitzi, D. B.; Kosbar, L. L.; Murray, C. E.; Copel, M.; Afzali, A. *Nature* **2004**, *428*, 299−303.

(26) Mitzi, D. B. *Inorg. Chem.* **2005**, *44*, 7078−7086.

(27) Milliron, D. J.; Mitzi, D. B.; Copel, M.; Murray, C. E. *Chem. Mater.* **2006**, *18*, 587−590.

(28) Mitzi, D. B. *Inorg. Chem.* **2007**, *46*, 926−931.

(29) Yuan, M.; Dirmyer, M.; Badding, J.; Sen, A.; Dahlberg, M.; Schiffer, P. *Inorg. Chem.* **2007**, *46*, 7238−7240.

(30) McCandless, B. E.; Shafarman, W. N. U.S. Patent 6 537 845, 2003.

(31) Miller, A.; Mackinnon, A.; Weaire, D. *Solid State Physics* **1981**, *36*, 119−175.